J. Fluid Mech. (2024), *vol*. 983, R2, doi:10.1017/jfm.2024.143

Structure and role of the pressure Hessian in regions of strong vorticity in turbulence

P.-F. Yang[1,2,3], H. Xu[3], A. Pumir[4,5,†] and G.W. He[1,2,†]

[1]The State Key Laboratory of Nonlinear Mechanics, Institute of Mechanics, Chinese Academy of Sciences, Beijing 100190, PR China

[2]School of Engineering Sciences, University of Chinese Academy of Sciences, Beijing 100049, PR China

[3]Center for Combustion Energy and School of Aerospace Engineering, Tsinghua University, 100084 Beijing, PR China

[4]Laboratoire de Physique, Ecole Normale Supérieure de Lyon, CNRS, Université de Lyon, Lyon F-69007, France

[5]Max Planck Institute for Dynamics and Self-Organization, Am Fassberg 17, Göttingen D-37077, Germany

(Received 6 November 2023; revised 9 January 2024; accepted 3 February 2024)

Amplification of velocity gradients, a key feature of turbulent flows, is affected by the non-local character of the incompressible fluid equations expressed by the second derivative (Hessian) of the pressure field. By analysing the structure of the flow in regions where the vorticity is the highest, we propose an approximate expression for the pressure Hessian in terms of the local vorticity, consistent with the existence of intense vortex tubes. Contrary to the often used simplification of an isotropic form for the pressure Hessian, which in effect inhibits vortex stretching, the proposed approximate form of the pressure Hessian enables much stronger vortex stretching. The prediction of the approximation proposed here is validated with results of direct numerical simulations of turbulent flows.

Key words: turbulence theory, turbulence modelling, vortex dynamics

1. Introduction

The main difficulties to understand three-dimensional incompressible turbulent flows arise from two intrinsic properties of fluid mechanics, namely nonlinearity and non-locality. Nonlinearity leads to the generation of small-scale structures in turbulent flows and to the intermittent formation of highly localized and intense velocity gradients (Taylor 1938).

† Email addresses for correspondence: alain.pumir@ens-lyon.fr, hgw@lnm.imech.ac.cn

It is well established that strong vorticity regions emerge, forming tube-like structures (Siggia 1981; She, Jackson & Orszag 1990; Jackson, She & Orszag 1991; Jiménez *et al.* 1993; Ishihara, Gotoh & Kaneda 2009; Buaria *et al.* 2019), surrounded by sheet-like structures of strong strain regions (Buaria *et al.* 2019; Buaria, Pumir & Bodenschatz 2021). Interestingly, the structural difference between regions of intense strain and intense vorticity results in a strong asymmetry: vorticity is large in regions of intense strain, but in comparison strain is not as strong in regions of intense vorticity (Buaria & Pumir 2022). On the other hand, the non-locality in turbulent flows is captured by the pressure field $p(\boldsymbol{x})$, which satisfies the Poisson equation:

$$\nabla^2 p = -\mathrm{tr}(\boldsymbol{m}^2), \tag{1.1}$$

where $\boldsymbol{m}$, the velocity gradient tensor, is defined by $m_{ij} \equiv \partial u_i/\partial x_j$, u being the fluid velocity. The classical solution of (1.1) leads to an expression of the pressure at any point as an integral of the velocity gradient over the whole space. The pressure field in turn enters the evolution equations for the velocity gradient tensor:

$$\frac{\mathrm{D}m_{ij}}{\mathrm{D}t} = -m_{ik}m_{kj} - h^p_{ij} + \nu\nabla^2 m_{ij}. \tag{1.2}$$

In (1.2), ν is the kinematic viscosity, and $h^p_{ij} \equiv \partial^2 p/\partial x_i \partial x_j$ the pressure Hessian tensor. A detailed understanding of the pressure Hessian is therefore a prerequisite to describe the dynamics of the velocity gradient tensor. Earlier studies have investigated the role of pressure Hessian in (1.2) (Borue & Orszag 1998; Tsinober, Ortenberg & Shtilman 1999; Carbone, Iovieno & Bragg 2020; Zhou & Yang 2023), or in the equation for the coarse-grained velocity gradient tensor (Chertkov, Pumir & Shraiman 1999; Yang, Pumir & Xu 2020; Tom, Carbone & Bragg 2021). An important issue consists in understanding the role of velocity gradient structure on pressure (Pumir 1994; Vlaykov & Wilczek 2019), and more generally, in developing closure models for the pressure Hessian in the Lagrangian dynamics of velocity gradient (Vieillefosse 1982, 1984; Cantwell 1992; Martın, Dopazo & Valiño 1998*a*; Martın *et al.* 1998*b*; Chevillard *et al.* 2008; Meneveau 2011; Wilczek & Meneveau 2014; Lawson & Dawson 2015; Johnson & Meneveau 2016; Tian, Livescu & Chertkov 2021). Here, our general objective is to propose an approximate expression for the pressure Hessian, using a closed expression in terms of the velocity gradient, with the aim of providing insight on the dynamics of the velocity gradient tensor itself.

The simplifying assumption, known as restricted Euler (RE), consists in considering an isotropic functional form for $\boldsymbol{h}^p$, i.e. $h^p_{ij} = \frac{1}{3}\nabla^2 p\delta_{ij}$, with δ_{ij} being the Kronecker symbol and $\nabla^2 p$ given by (1.1). This approximate form expresses $\boldsymbol{h}^p$ locally in terms of strain and vorticity, and is formally obtained by neglecting non-local contributions when expressing the solution of (1.1) (Ohkitani & Kishiba 1995). Remarkably, this leads to a simple dynamical system which can be integrated with elementary means (Vieillefosse 1982, 1984; Cantwell 1992), therefore providing a qualitative dynamics, in a statistical sense, in the (R, Q) plane, where $R \equiv -\frac{1}{3}\mathrm{tr}(\boldsymbol{m}^3)$ and $Q \equiv -\frac{1}{2}\mathrm{tr}(\boldsymbol{m}^2)$ are two invariants of $\boldsymbol{m}$. In particular, the simplified dynamics leads to a singularity along the separatrix $4Q^3 + 27R^2 = 0$ and $R > 0$, which provides an explanation for the excess of probability of the invariants along this separatrix (Cantwell 1993). However, the RE assumption predicts that in vorticity-dominated regions ($Q > 0$), the flow moves quickly away from regions with positive vortex stretching ($R < 0$) towards regions where vortex stretching is negative. In comparison, the results of direct numerical simulation (DNS) show that the approximate form of the pressure Hessian obtained from the RE approximation leads

to an excessively strong inhibition of vortex stretching (Tsinober 2009; Buaria & Pumir 2023). This clearly implies that the deviatoric part of h_{ij}^p, denoted H_{ij}^p in the following, and defined as the difference between the pressure Hessian and the isotropic component, $\frac{1}{3}\nabla^2 p\delta_{ij}$: $H_{ij}^p \equiv h_{ij}^p - \frac{1}{3}\nabla^2 p\delta_{ij}$, plays an essential role. The difficulty, however, is that H_{ij}^p is determined by an integral expression (Ohkitani & Kishiba 1995).

Here, we focus on regions with strong vorticity, and propose that the pressure Hessian tensor is determined primarily by local vorticity values due to the asymmetric distribution of vorticity and strain. We will present our theory and propose that

$$\frac{\partial^2 p}{\partial x_i \partial x_j} \approx -\frac{1}{3}\mathrm{tr}(\boldsymbol{m}^2)\delta_{ij} - \frac{1}{4}\left(\omega_i\omega_j - \frac{1}{3}\omega^2\delta_{ij}\right) \quad \text{when } \Omega\tau_K^2 \gg 1, \tag{1.3}$$

where $\omega_i \equiv \epsilon_{ijk}m_{jk}$ is the vorticity (ϵ_{ijk} is the Levi–Civita tensor) and $\Omega \equiv \omega_i\omega_i$ is twice the enstrophy, and $\tau_K \equiv 1/\langle\Omega\rangle^{1/2}$ denotes the Kolmogorov time scale. Throughout this text, $\langle\cdot\rangle$ denotes the ensemble average of a fluctuating quantity. We then discuss the implications of this result on the Lagrangian dynamics of the velocity gradient. Our analysis shows that the contributions from the deviatoric parts of pressure Hessian are not negligible and counteract the contribution of nonlinear terms to the leading order, and leads to an enhancement of vortex stretching in moderately strong vorticity regions.

2. The DNS data

We first introduce the two DNS datasets of homogeneous and isotropic turbulence used in this work. Dataset A is downloaded from snapshot 5 of the 'Forced isotropic turbulence dataset on 8192^3 Grid' dataset (Yeung, Zhai & Sreenivasan 2015; Yeung, Sreenivasan & Pope 2018) of the Johns Hopkins turbulence database (Li *et al.* 2008), with 8192^3 grid points and a Taylor-microscale based Reynolds number $R_\lambda = 610$. The spatial resolution is characterized by $k_{max}\eta_K \approx 5.3$, where k_{max} is the largest resolved wavenumber and η_K is the Kolmogorov scale. To study the properties of the pressure Hessian conditioned on extreme values of vorticity, we use the 'GetThreshold' function of the database and downloaded all data points with $\Omega\tau_K^2 > 24.98$. Because of the limited storage space, we only keep the points with $24.98 < \Omega\tau_K^2 < 25.02$, $99 < \Omega\tau_K^2 < 101$ and $\Omega\tau_K^2 > 196$. Then the statistic for $\Omega\tau_K^2 = 25$ would be 2.3×10^6, and 2.2×10^6 for $\Omega\tau_K^2 = 100$. For comparison, we also downloaded 512^3 equally spaced data points of the whole snapshot, which would provide information for statistics of unconditional and lower values of vorticity.

Dataset B was obtained by simulating the Navier–Stokes equations using the spectral code described in Pumir (1994) with 512^3 grid points and $R_\lambda = 210$, with a lower spatial resolution compared with Dataset A: $k_{max}\eta_K \approx 1.6$. While this resolution is insufficient to reliably capture the statistics of the largest velocity gradients in the flow, we explicitly checked that the probability density function (p.d.f.) of enstrophy, Ω, coincides with the data shown in figure 2 of Buaria *et al.* (2019) at $R_\lambda = 240$, for $\Omega\tau_K^2 \lesssim 50$. Other tests convinced us that resolution is not an issue over the range of velocity gradient intensity considered here. We saved 21 configurations of the full velocity fields, over a time of the order of $\sim$10 eddy turnover times, which we analysed to produce the data shown here.

3. Analysis of the pressure Hessian in regions of very large vorticity

We begin by focusing on the antisymmetric part of the velocity gradient tensor in (1.2), which involves vorticity $\boldsymbol{\omega}$ and thus the enstrophy Ω:

$$\frac{1}{2}\frac{\mathrm{D}\Omega}{\mathrm{D}t} = \omega_i s_{ij}\omega_j + \nu\omega_i\nabla^2\omega_i, \tag{3.1}$$

where $s_{ij} \equiv \frac{1}{2}(m_{ij} + m_{ji})$ is the rate of strain tensor. Equation (3.1) implies that enstrophy amplification results from a competition between vortex stretching $\omega_i s_{ij}\omega_j$ and the viscous diffusion. Notoriously, the pressure Hessian does not explicitly appear in the equations for ω_i and Ω. On the other hand, the pressure Hessian $\partial^2 p/\partial x_i\partial x_j$ plays an explicit role in the dynamic equation of strain s_{ij}:

$$\frac{\mathrm{D}s_{ij}}{\mathrm{D}t} = -s_{ik}s_{kj} - \frac{1}{4}\left(\omega_i\omega_j - \omega^2\delta_{ij}\right) - h^p_{ij} + \nu\nabla^2 s_{ij}, \tag{3.2}$$

and, therefore, pressure Hessian will affect the vortex stretching dynamics by acting on strain (Buaria & Pumir 2023).

3.1. *Heuristic derivation*

We start by conditioning the equation of the dynamics of strain, (3.2), on enstrophy Ω and taking the conditional average:

$$\left\langle\frac{\mathrm{D}s_{ij}}{\mathrm{D}t}|\Omega\right\rangle + \left\langle s_{ik}s_{kj}|\Omega\right\rangle + \left\langle\frac{1}{4}\left(\omega_i\omega_j - \omega^2\delta_{ij}\right)|\Omega\right\rangle + \left\langle h^p_{ij}|\Omega\right\rangle - \left\langle\nu\nabla^2 s_{ij}|\Omega\right\rangle = 0. \tag{3.3}$$

Earlier work has shown that vorticity dominates the strain in extreme vorticity regions, in the sense that $\langle\Sigma|\Omega\rangle \sim \Omega^\gamma$, with $\Sigma \equiv 2s_{ij}s_{ji}$, and with $\gamma < 1$ when $\Omega\tau_K^2 \gg 1$ (Buaria *et al.* 2019; Buaria, Bodenschatz & Pumir 2020; Buaria & Pumir 2022). We use the corresponding feature, namely $\Sigma \ll \Omega$, to analyse the magnitudes of the various terms appearing in (3.3). This is at the origin of the simple functional form for h^p_{ij} that we propose in this work.

We first notice that both the operators $\mathrm{D}/\mathrm{D}t$ and $\nu\nabla^2$ have the dimension of the inverse of a time, $1/T$. Given that the fastest time scale in extreme vorticity regions is $1/\Omega^{1/2}$, we estimate that

$$\left\langle\frac{\mathrm{D}s_{ij}}{\mathrm{D}t}|\Omega\right\rangle, \quad \left\langle\nu\nabla^2 s_{ij}|\Omega\right\rangle \lesssim \Sigma^{1/2}\Omega^{1/2}. \tag{3.4a,b}$$

Besides, the second and third terms on the left-hand side of (3.3) scale as

$$\left\langle s_{ik}s_{kj}|\Omega\right\rangle \sim \Sigma \ll \left\langle\frac{1}{4}\left(\omega_i\omega_j - \omega^2\delta_{ij}\right)|\Omega\right\rangle \sim \Omega. \tag{3.5}$$

Thus the third term dominates the first, second and fifth terms on the left-hand side of (3.3), as a result, we should have $\langle h^p_{ij}|\Omega\rangle \sim \langle -\frac{1}{4}(\omega_i\omega_j - \omega^2\delta_{ij})|\Omega\rangle$ when $\Omega\tau_K^2 \gg 1$. This argument suggests that the pressure Hessian is determined by the local value of vorticity in extreme vorticity regions. For simplicity, we denote $\tilde{h}^p_{ij} \equiv -\frac{1}{4}(\omega_i\omega_j - \omega^2\delta_{ij})$ and, subtracting out the trace, we obtain its deviatoric part as

$$\tilde{H}^p_{ij} \equiv -\frac{1}{4}\left(\omega_i\omega_j - \tfrac{1}{3}\omega^2\delta_{ij}\right). \tag{3.6}$$

The approximations leading to (3.6) suggest that the difference between H^p_{ij} and $\tilde{H}^p_{ij}$ is mostly due to the strain component, which is explicitly neglected in our heurstic derivation.

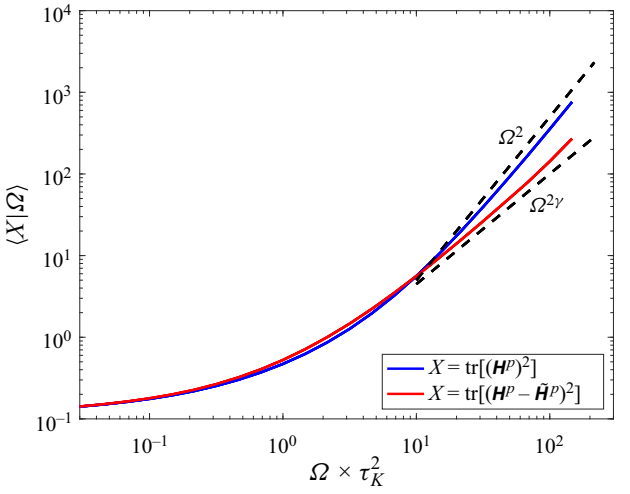

Figure 1. Second moment of the deviatoric part of the pressure Hessian tensor, $\boldsymbol{H}^p$ (blue line) and of the difference, $(\boldsymbol{H}^p - \tilde{\boldsymbol{H}}^p)$ (red line) conditioned on Ω. In agreement with the approximation proposed in the text, the second moment of $\boldsymbol{H}^p$ grows as Ω^2, whereas the second moment of $(\boldsymbol{H}^p - \tilde{\boldsymbol{H}}^p)$ grows as $\Omega^{2\gamma}$, with $\gamma < 1$. Dataset B was used to construct the figure.

This is consistent with our own numerical results, see e.g. figure 1, which indicate that the average of $\mathrm{tr}[(\boldsymbol{H}^p - \tilde{\boldsymbol{H}}^p)^2]$ conditioned on Ω grows as $\sim\Omega^{2\gamma}$, whereas the average of $\mathrm{tr}[(\boldsymbol{H}^p)^2]$ conditioned on Ω grows as $\sim \Omega^2$. This implies, in particular, that the p.d.f. of the difference between $\boldsymbol{H}^p$ and its asymptotic form is becoming narrower, in units of $\langle \mathrm{tr}[(\boldsymbol{H}^p)^2]|\Omega\rangle$ when Ω is very large.

3.2. *Structure of the pressure Hessian in regions of large vorticity*

Before exploring the implications of (3.6) on the dynamics of the velocity gradient tensor, we first discuss the properties of the tensor $\tilde{\boldsymbol{H}}^p$, and compare them with the results of DNS.

It is easy to see that the tensor $\tilde{h}^p_{ij} = -\frac{1}{4}(\omega_i\omega_j - \omega^2\delta_{ij})$ has a zero eigenvalue in the eigendirection $\hat{\boldsymbol{\omega}}$, along with a degenerate eigenvalue $\frac{1}{4}\omega^2$, in the plane perpendicular to $\hat{\boldsymbol{\omega}}$. This is generally consistent with DNS results. Nomura & Post (1998), Lawson & Dawson (2015) and Buaria & Pumir (2023) observed that when $\Omega\tau_K^2 \gg 1$, $\hat{\boldsymbol{\omega}}$ strongly aligns with eigendirection $\boldsymbol{e}_3^{ph}$ of the pressure Hessian h^p_{ij}; and the largest and the smallest eigenvalues of h^p_{ij} conditioned on large Ω tend to approach $\frac{1}{4}\omega^2$ and 0; the intermediate one reaching a value slightly smaller than $\frac{1}{4}\omega^2$. To investigate further the structure of the eigenvalues of $\boldsymbol{h}^p$, we study the joint p.d.f. of its invariants. Following Tom *et al.* (2021), we define

$$b_{ij} \equiv \left(h^p_{ij} - \tfrac{1}{3}\delta_{ij}h^p_{kk}\right) \Big/ \sqrt{h^p_{ln}h^p_{ln}}, \tag{3.7}$$

where $\boldsymbol{b}$ is the deviatoric part of the pressure Hessian, H^p_{ij}, normalized by the norm of $\boldsymbol{h}^p$. Furthermore, we construct the invariants of $\boldsymbol{b}$ as

$$\zeta = -\sqrt{6}\,\mathrm{tr}(\boldsymbol{b}^3), \quad \chi = \left(\mathrm{tr}(\boldsymbol{b}^2)\right)^{3/2}. \tag{3.8a,b}$$

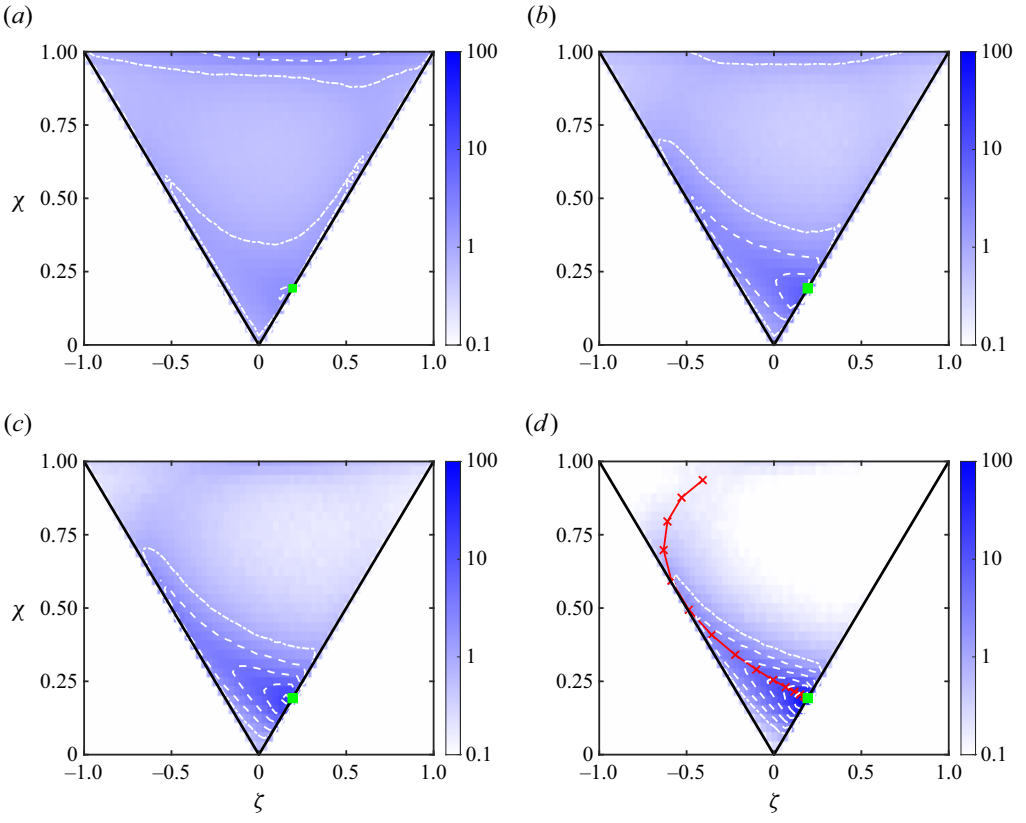

Figure 2. Joint p.d.f. of the dimensionless invariants ζ and χ of the pressure Hessian conditioned on (*a*) $\Omega\tau_K^2 = 1$, (*b*) $\Omega\tau_K^2 = 4$, (*c*) $\Omega\tau_K^2 = 25$ and (*d*) $\Omega\tau_K^2 = 100$. The red line with cross symbols in (*d*) corresponds to a Burgers vortex. The white dashed-dotted lines show the iso-probability contours corresponding to the value 1, and the dashed lines to 2^n.

Figure 2 shows the joint p.d.f. of ζ and χ for $\Omega\tau_K^2 = 1$, 4, 25 and 100, respectively. The eigenvalues of the pressure Hessian exhibit a high-probability region near the configuration corresponding to $\tilde{h}_{ij}^p$, where $\lambda_1^p = \lambda_2^p = h_{ii}^p/2$ and $\lambda_3^p = 0$ so $\chi = \zeta = \sqrt{3}/9 \approx 0.1925$. This configuration is indicated by the green squares in figure 2.

We now demonstrate that the structure of the p.d.f.s of (ζ, χ) conditioned on $\Omega\tau_K^2 \gg 1$ is fully consistent with the presence of intense vortex tube-like structure (Siggia 1981; She *et al.* 1990; Jiménez *et al.* 1993; Ishihara *et al.* 2009; Buaria *et al.* 2019). To this end, we consider a Burgers vortex, characterized by the standard definition of the Reynolds number, $Re = \Gamma/\nu$, where Γ is the circulation of the vortex. At the centre of the vortex (Burgers 1948) with $Re \gg 1$, the eigenvalues of the pressure Hessian are also $\frac{1}{4}\omega^2$, $\frac{1}{4}\omega^2$ and 0; and the eigendirection corresponding to the 0 eigenvalue aligns with $\hat{\boldsymbol{\omega}}$ (Andreotti 1997; Horiuti 2001; Horiuti & Takagi 2005). We now compare the structure of the pressure Hessian in a turbulent flow with that in a Burgers vortex, whose properties depend only on the distance r to the axis. Following Andreotti (1997), we use the dimensionless radius $r^* = r\,a/\nu$, where a is the external strain rate acting on the vortex. We note that the Reynolds number Re amounts to the vorticity at the centre divided by the external strain a. As already stated, the maximum value of the probability in all panels of figure 2, indicated by the green squares, corresponds to the axisymmetric configuration on the axis of the

vortex ($r^* = 0$). Furthermore, the dependence of the invariants ζ and χ on r^* up to $r^* = 1$ in a Burgers vortex is shown as the red line with crosses in figure 2(*d*), see also (4) of Andreotti (1997). As r^* increases, the solution moves up in the (ζ, χ) plane, first towards the left border and then back towards the centre. We note that its variation with respect to Reynolds number Re is negligible. The joint p.d.f. of (ζ, χ), particularly the ridges, closely follows the Burgers vortex solution. We also observe that when conditioning on a given value of $\Omega\tau_K^2$, as done in figure 2, the points at a given value of (ζ, χ) away from the maximum, or $\zeta = \chi = \sqrt{3}/9$, correspond to points at some distances away from the centre, or $r^* > 0$, of vortices with increasing intensity. These vortices are therefore less probable, which explains that the maximum probability in figure 2 corresponds to $\zeta = \chi = \sqrt{3}/9$. Additionally, the distribution becomes more concentrated along the red curve when $\Omega\tau_K^2$ increases. Figure 2 therefore demonstrates that the Burgers vortex model provides a compelling qualitative description of the pressure Hessian. We notice, however, that any axisymmetric vortex model would lead to qualitatively similar observations near the centre of the vortex, consistent with (3.6) for the deviatoric part of the pressure Hessian tensor.

4. Dynamics in the (R, Q) plane

To illustrate the dynamical implications of (3.6), we project the equations of motion for $\boldsymbol{m}$ on the plane (R, Q), where the invariants R and Q are defined by

$$Q \equiv -\tfrac{1}{2} m_{ij} m_{ji} = -\tfrac{1}{2} s_{ij} s_{ji} + \tfrac{1}{4}\omega^2, \tag{4.1}$$

$$R \equiv -\tfrac{1}{3} m_{ij} m_{jk} m_{ki} = -\tfrac{1}{3} s_{ij} s_{jk} s_{ki} - \tfrac{1}{4}\omega_i s_{ij} \omega_j. \tag{4.2}$$

In (4.1) and (4.2), and throughout this text, we assume summation of repeated indices. Physically, Q expresses the difference between enstrophy and the square of the strain rate, so $Q = \frac{1}{2}\Omega - \mathrm{tr}(\boldsymbol{s}^2) > 0$ corresponds to vorticity-dominated regions and $Q < 0$ corresponds to strain-dominated regions. Similarly, $R = -\frac{1}{3}\mathrm{tr}(\boldsymbol{s}^2) - \frac{1}{4}\boldsymbol{\omega}\cdot\boldsymbol{s}\cdot\boldsymbol{\omega} < 0$ corresponds to the vortex-stretching-dominated region. The exact Lagrangian evolution equations for the invariants R and Q can be readily derived from (1.2):

$$\frac{\mathrm{d}Q}{\mathrm{d}t} = -3R + m_{ij} H^p_{ji} - m_{ij} H^\nu_{ji}, \tag{4.3}$$

$$\frac{\mathrm{d}R}{\mathrm{d}t} = \frac{2}{3}Q^2 + m_{ij} m_{jk} H^p_{ki} - m_{ij} m_{jk} H^\nu_{ki}, \tag{4.4}$$

where H^p_{ij} is the deviatoric part of the pressure Hessian, and $H^\nu_{ij} \equiv \nu(\partial^2 m_{ij}/\partial x_k \partial x_k)$. We stress that these two terms in (4.3) and (4.4) are unclosed. The RE approximation introduced above provides a closure consisting in neglecting the deviatoric contributions to the pressure Hessian: $\boldsymbol{H}^p = \boldsymbol{0}$. As mentioned already (Buaria & Pumir 2023), the RE assumption fails to predict the qualitative behaviour of the dynamics in the (R, Q) plane when Q is positive and large. Specifically, the RE assumption leads to $\mathrm{d}R/\mathrm{d}t = \frac{2}{3}Q^2 > 0$, but the results of DNS show that $\mathrm{d}R/\mathrm{d}t < 0$ in some region of the second quadrant of the (R, Q) plane, see, for example, figures 3(*a*) and 3(*d*) of Wilczek & Meneveau (2014) and figure 5 of Yang *et al.* (2023). The observation that pressure leads to a 'depression of nonlinearity' (Borue & Orszag 1998) suggests the functional $H^p_{ij} = -\alpha(m_{ik}m_{kj} - \frac{1}{3}\mathrm{tr}(\boldsymbol{m}^2)\delta_{ij})$ where $0 < \alpha < 1$ is a model parameter (Chertkov *et al.* 1999). This model predicts that the pressure terms induced by H^p_{ij} in (4.3) and (4.4) anti-align with the RE

terms in the (R, Q) plane, in quantitative contradiction with numerical results for $Q > 0$, and particularly for $R < 0$. Attempts to improve the RE approximation have assumed mostly some local expressions for the pressure Hessian, with an explicit relation between $\boldsymbol{H}^p$ and the velocity gradient tensor $\boldsymbol{m}$ (Wilczek & Meneveau 2014). In the following, we will discuss theoretically the role of pressure Hessian in the vorticity-dominated regions, and derive a local analytical expression for the contributions of H^p_{ij} in Eqs. (4.3) and (4.4), to leading order when $\Omega\tau_K^2 \gg 1$.

We now use the approximate form of the deviatoric part of the pressure Hessian, (3.6), to analyse the dynamics in the (R, Q) plane. When $\Omega\tau_K^2 \gg 1$, (3.6) gives

$$m_{ij}\tilde{H}^p_{ji} = -\tfrac{1}{4}\omega_i s_{ij}\omega_j = R - \tfrac{1}{3}s_{ij}s_{jk}s_{ki}, \tag{4.5}$$

$$m_{ij}m_{jk}\tilde{H}^p_{ki} = -\tfrac{2}{3}Q^2 - \tfrac{1}{12}\omega^2 s_{ij}s_{ji} + \tfrac{1}{6}(s_{ij}s_{ji})^2 - \tfrac{1}{4}\omega_i s_{ik}s_{kj}\omega_j. \tag{4.6}$$

We recall that the expressions for $\mathrm{d}Q/\mathrm{d}t$ and $\mathrm{d}R/\mathrm{d}t$ obtained by using the RE approximation, provided by (4.3) and (4.4) are $-3R$ and $\frac{2}{3}Q^2$, respectively. In the spirit of the approach in § 3.1, based on the quantitative difference between Σ and Ω, namely with $\Sigma \ll \Omega$ when $\Omega\tau_K^2 \gg 1$, we further notice that when $\Omega\tau_K^2 \gg 1$, $R \gg \frac{1}{3}s_{ij}s_{jk}s_{ki}$, so the $\boldsymbol{H}^p$ term cancels, to the leading order in Σ/Ω, approximately 1/3 of the RE term in the Q equation. More significantly, in the limit $\Omega\tau_K^2 \gg 1$, we find that $Q^2 \gg \omega^2 s_{ij}s_{ji}$, $\omega_i s_{ik}s_{kj}\omega_j \gg (s_{ij}s_{ji})^2$ in the R equation, so the $\boldsymbol{H}^p$ terms cancel out the dominant RE term $\frac{2}{3}Q^2$. The lowest-order contribution in a formal development in (Σ/Ω) involves terms such as $-\frac{1}{12}\omega^2 s_{ij}s_{ji} - \frac{1}{4}\omega_i s_{ik}s_{kj}\omega_j$, which is negative. We observe that this implies $\mathrm{d}R/\mathrm{d}t < 0$, which is generally consistent with the DNS results (see e.g. figure 5 of Yang *et al.* 2023). Earlier work aimed at describing the pressure Hessian (Chevillard *et al.* 2008; Wilczek & Meneveau 2014) did not particularly focus on high-enstrophy regions. It would be interesting to compare the corresponding predictions in light of the approximation. We note that the tetrad model (Chertkov *et al.* 1999; Yang *et al.* 2020, 2023) involves quadratic terms in the vorticity introduced through the full tensor $\boldsymbol{m}$, insufficient to compensate for the strong vortex-stretching reduction due to the RE approximation.

Figure 3(*a*) shows the DNS results for $\mathrm{d}Q/\mathrm{d}t$ and $\mathrm{d}R/\mathrm{d}t$ on the (R, Q) plane (blue arrows) and compares them with the theoretical predictions (magenta arrows). Figure 3(*a*) demonstrates that when $Q\tau_K^2 \gtrsim 5$ and $|R\,\tau_K^3|$ is not too large, the magenta arrows, which represent our theoretical predictions (rightmost terms of (4.5), (4.6)), agree well with the blue arrows, which represent the 'exact' DNS values. Figure 3 also directly compares the ratios between the numerically determined values $\mathrm{tr}(\boldsymbol{H}^p \cdot \boldsymbol{m})$ (*b*) and $\mathrm{tr}(\boldsymbol{H}^p \cdot \boldsymbol{m}^2)$ (*c*) and the values found by replacing $\boldsymbol{H}^p$ by $\tilde{\boldsymbol{H}}^p$. The agreement for the $\mathrm{tr}(\boldsymbol{H}^p \cdot \boldsymbol{m}^2)$ generally improves when Q increases, as expected when $\Omega\tau_K^2$ increases. The effect is weaker for the term $\mathrm{tr}(\boldsymbol{H}^p \cdot \boldsymbol{m})$. We note that the quality of the agreement at $R \approx 0$ degrades when $Q\tau_K^2$ increases, which is due to the small values of both numerator and denominator. Figure 4 provides further insight on the dynamics, by comparing the contributions of $\boldsymbol{H}^p$ to $\mathrm{d}Q/\mathrm{d}t$ and $\mathrm{d}R/\mathrm{d}t$ in the (R, Q) plane, with the leading-order terms in (4.5) and (4.6), namely R and $-\frac{2}{3}Q^2$. Figure 4 reveals that when $Q\tau_K^2 > 5$ and $|R\tau_K^3|$ is not too large, the green arrows, which represent our theoretical predictions to leading order are reassuringly close to the blue arrows, which represent the values obtained directly from DNS.

Remarkably, we notice that using $-\frac{2}{3}Q^2$ for the contribution due to the deviatoric part of the pressure Hessian leads to $\mathrm{d}R/\mathrm{d}t = 0$ in the inviscid case. Whether the blue arrows in figure 4(*a*) are longer or shorter than the green ones in fact determines the sign of $\mathrm{d}R/\mathrm{d}t$. We observe that $\mathrm{d}R/\mathrm{d}t > 0$ when $Q\tau_K^2 \gtrsim 20$ for Dataset B with $R_\lambda = 210$. At lower values

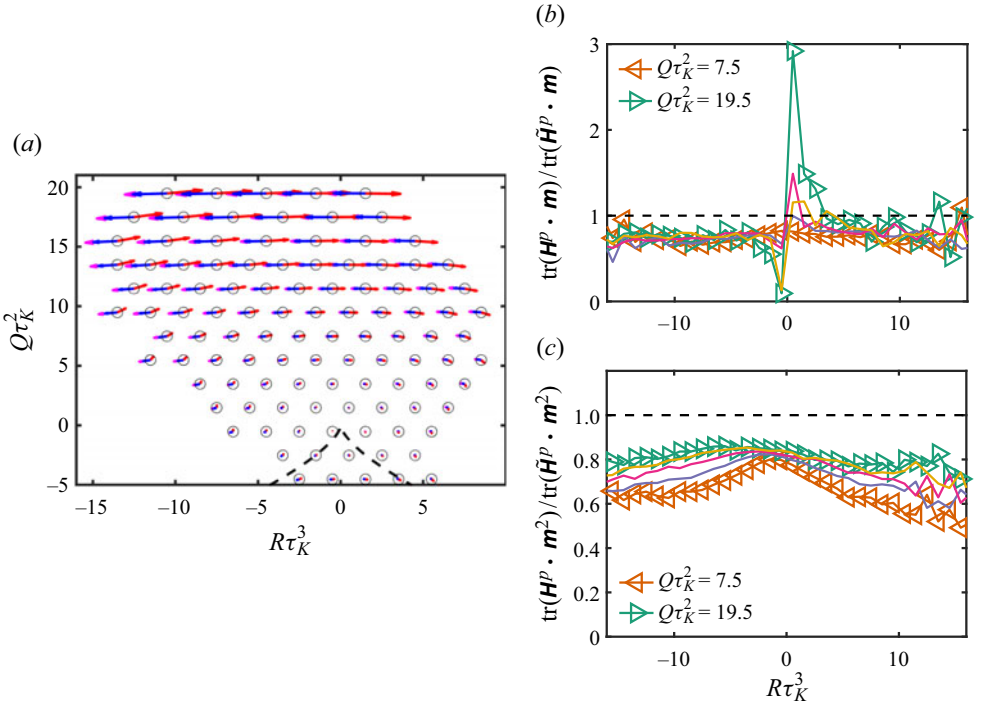

Figure 3. (*a*) Results for $\mathrm{d}Q/\mathrm{d}t$ and $\mathrm{d}R/\mathrm{d}t$ in the (R, Q) plane. The red arrows show the RE term $(-3R, \frac{2}{3}Q^2)$, the blue arrows the deviatoric pressure Hessian term $(-m_{ij}H^p_{ji}, -m_{ij}m_{jk}H^p_{ki})$ and the magenta arrows our theoretical predictions for large Ω, i.e. the rightmost terms of (4.5), (4.6). Panels (*b*,*c*) show the ratio between the contributions of the deviatoric part of the pressure Hessian, $\boldsymbol{H}^p$, and those of the approximate form, $\tilde{\boldsymbol{H}}^p$, (3.6), to $\mathrm{d}Q/\mathrm{d}t$ (*b*) and $\mathrm{d}R/\mathrm{d}t$ (*c*). The ratios, plotted as a function of $R\tau_K^3$, increase towards 1 as $Q\tau_K^2$ increases. The large value for $\mathrm{d}Q/\mathrm{d}t$ close to $R\tau_K^3 \approx 0$ corresponds to very small values of both the terms $\mathrm{tr}(\boldsymbol{H}^p \cdot \boldsymbol{m})$ and $\mathrm{tr}(\tilde{\boldsymbol{H}}^p \cdot \boldsymbol{m})$. Dataset B was used to construct the figure.

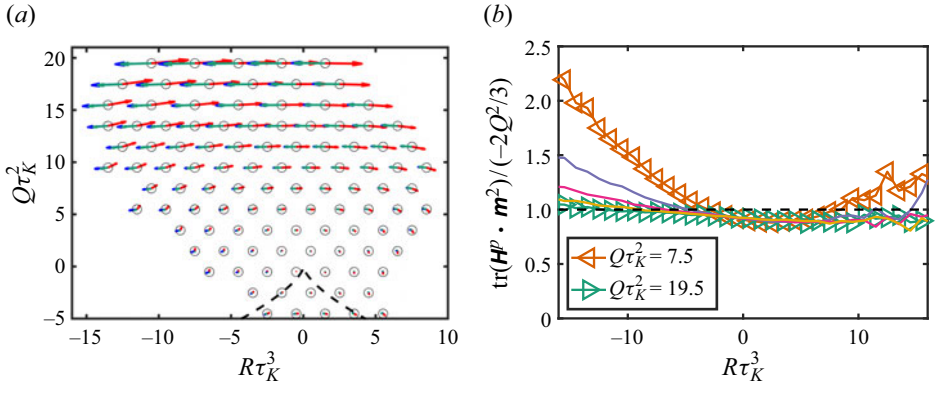

Figure 4. (*a*) Pressure contribution to $\mathrm{d}Q/\mathrm{d}t$ and $\mathrm{d}R/\mathrm{d}t$ in the (R, Q) plane. The red arrows correspond to the RE term $(-3R, \frac{2}{3}Q^2)$, which corresponds to the isotropic (local) contribution of the pressure Hessian, the blue arrows to the anisotropic pressure Hessian term $(-m_{ij}H^p_{ji}, -m_{ij}m_{jk}H^p_{ki})$ and the green arrows show the simplified theoretical predictions at large Ω, $(R, -\frac{2}{3}Q^2)$. Panel (*b*) shows the ratio between the contribution of $\boldsymbol{H}^p$ to $\mathrm{d}R/\mathrm{d}t$, compared with the simplified form $-2Q^2/3$. Dataset B ($R_\lambda = 210$) was used to construct the figure.

of $Q\tau_K^2$, and for $R\tau_K^3$ sufficiently negative, on the contrary, $\mathrm{d}R/\mathrm{d}t < 0$. For these values, the dynamics tends to keep the values (R, Q) in the $(R < 0, Q > 0)$ quadrant, where stretching is largest. This contrasts sharply with the predictions of the RE approximation, which tends to inhibit vortex stretching (Buaria & Pumir 2023). A more precise comparison between $\mathrm{tr}(\boldsymbol{H}^p \cdot \boldsymbol{m}^2)$ and $-\frac{2}{3}Q^2$ is shown in figure 4(*b*). At relatively low value of $Q\tau_K^2$, and for $R\tau_K^3 \lesssim -3$, $\mathrm{tr}(\boldsymbol{H}^p \cdot \boldsymbol{m}^2)$ is more negative than $-\frac{2}{3}Q^2$, consistent with the observation that $\mathrm{d}R/\mathrm{d}t < 0$. As $Q\tau_K^2$ increases, however, the region where $\mathrm{d}R/\mathrm{d}t < 0$ is restricted to much larger values of $R\tau_K^3 < 0$, whereas at small, intermediate values of $|R\tau_K^3|$, $\mathrm{d}R/\mathrm{d}t > 0$.

5. Conclusion

In this work, we have proposed a very simple approximate expression for the deviatoric part of the pressure Hessian in terms of the local field, valid in regions of very large vorticity in turbulent flows. Namely, we find that $\partial^2 p/\partial x_i \partial x_j \sim -\frac{1}{4}(\omega_i\omega_j - \omega^2\delta_{ij})$ when $\omega^2\tau_K^2 \gg 1$. This simple expression comes from an elementary analysis of the flow, and in particular, on the structure of the solutions (vortex tubes) in these flow regions. We stress that the deviatoric term of the pressure Hessian is essentially non-local, which implies that (3.6) can be only approximately valid. Despite these limitations, the observations from DNS support our theoretical discussions and provide further evidence for our conclusions. The numerical results in homogeneous isotropic flows presented here therefore demonstrate that the considerations developed in this work provide potentially valuable insight into the closure models of pressure Hessian in the Lagrangian dynamics of velocity gradient. Although one expects on general grounds that our conclusions should extend to other turbulent flows, e.g. in the presence of mean shear and/or walls at large Reynolds numbers, it will be interesting to check the validity of our approximation for other classes of turbulent flows.

The expression (3.6) reduces to the simple explicit (local) relation between $\tilde{\boldsymbol{H}}^p_{ij}$ and $w_{ij} \equiv \frac{1}{2}(m_{ij} - m_{ji})$, the antisymmetric part of the velocity gradient tensor: $\tilde{H}^p_{ij} = w_{ik}w_{kj} - \frac{1}{3}\mathrm{tr}(\boldsymbol{w}^2)\delta_{ij}$. We note in this respect that recent machine-learning approaches (Tian *et al.* 2021; Buaria & Sreenivasan 2023) have looked systematically for an expansion of $\boldsymbol{H}^p$ in terms of all the invariants of the velocity gradient tensor, $\boldsymbol{m}$. In this sense, (3.6) can be compared with that from machine learning approaches. Alternatively, the expression provides a point of comparison which may be used in a physics-informed machine-learning approach. It is our expectation that the physical considerations initiated in this work can be further developed, and can lead to clearer understanding of the structure and modelling of turbulent flows.

Funding. P.-F.Y., H.X. and G.W.H. are grateful to the Natural Science Foundation of China (NSFC) Basic Science Center Program 'Multiscale Problems in Nonlinear Mechanics' (grant no. 11988102). P.-F.Y. and H.X. also acknowledge financial support from the NSFC grants 12202452, 11672157 and 91852104. A.P. received support from Agence Nationale de la Recherche (ANR) under grant number Contract TILT No. ANR-20-CE30-0035.

Declaration of interests. The authors report no conflict of interest.

Author ORCIDs.
P.-F. Yang https://orcid.org/0000-0003-1949-500X;
H. Xu https://orcid.org/0000-0002-2863-7658;
A. Pumir https://orcid.org/0000-0001-9946-7353;
G.W. He https://orcid.org/0000-0003-4738-0816.

References

Andreotti, B. 1997 Studying Burgers' models to investigate the physical meaning of the alignments statistically observed in turbulence. *Phys. Fluids* **9**, 735–742.

Borue, V. & Orszag, S.A. 1998 Local energy flux and subgrid-scale statistics in three-dimensional turbulence. *J. Fluid Mech.* **366**, 1–31.

Buaria, D., Bodenschatz, E. & Pumir, A. 2020 Vortex stretching and enstrophy production in high Reynolds number turbulence. *Phys. Rev. Fluids* **5**, 104602.

Buaria, D. & Pumir, A. 2022 Vorticity-strain rate dynamics and the smallest scales of turbulence. *Phys. Rev. Lett.* **128**, 094501.

Buaria, D. & Pumir, A. 2023 Role of pressure in generation of intense velocity gradients in turbulence. *J. Fluid Mech.* **973**, A23.

Buaria, D., Pumir, A. & Bodenschatz, E. 2021 Generation of intense dissipation in high Reynolds number turbulence. *Phil. Trans. R. Soc. Lond.* A **380**, 20210088.

Buaria, D., Pumir, A., Bodenschatz, E. & Yeung, P.K. 2019 Extreme velocity gradients in turbulent flows. *New J. Phys.* **21**, 043004.

Buaria, D. & Sreenivasan, K.R. 2023 Forecasting small-scale dynamics of fluid turbulence using deep neural networks. *Proc. Natl Acad. Sci. USA* **120**, 30.

Burgers, J.M. 1948 A mathematical model illustrating the theory of turbulence. *Adv. Appl. Mech.* **1**, 171–199.

Cantwell, B.J. 1992 Exact solution of a restricted Euler equation for the velocity gradient tensor. *Phys. Fluids* A **4**, 782–793.

Cantwell, B.J. 1993 On the behavior of velocity gradient tensor invariants in direct numerical simulations of turbulence. *Phys. Fluids* A **5**, 2008–2013.

Carbone, M., Iovieno, M. & Bragg, A.D. 2020 Symmetry transformation and dimensionality reduction of the anisotropic pressure Hessian. *J. Fluid Mech.* **900**, A38.

Chertkov, M., Pumir, A. & Shraiman, B.I. 1999 Lagrangian tetrad dynamics and the phenomenology of turbulence. *Phys. Fluids* **11**, 2394–2410.

Chevillard, L., Meneveau, C., Biferale, L. & Toschi, F. 2008 Modeling the pressure Hessian and viscous Laplacian in turbulence: comparisons with direct numerical simulation and implications on velocity gradient dynamics. *Phys. Fluids* **20**, 101504.

Horiuti, K. 2001 A classification method for vortex sheet and tube structures in turbulent flows. *Phys. Fluids* **13**, 3756–3774.

Horiuti, K. & Takagi, Y. 2005 Identification method for vortex sheet structures in turbulent flows. *Phys. Fluids* **17**, 121703.

Ishihara, T., Gotoh, T. & Kaneda, Y. 2009 Study of high Reynolds number isotropic turbulence by direct numerical simulation. *Annu. Rev. Fluid Mech.* **41**, 165–180.

Jackson, E., She, Z.-S. & Orszag, S.A. 1991 A case study in parallel computing: I. Homogeneous turbulence on a hypercube. *J. Sci. Comput.* **6**, 27–45.

Jiménez, J., Wray, A.A., Saffman, P.G. & Rogallo, R.S. 1993 The structure of intense vorticity in isotropic turbulence. *J. Fluid Mech.* **255**, 65–90.

Johnson, P.L. & Meneveau, C. 2016 A closure for Lagrangian velocity gradient evolution in turbulence using recent-deformation mapping of initially Gaussian fields. *J. Fluid Mech.* **804**, 387–419.

Lawson, J.M. & Dawson, J.R. 2015 On velocity gradient dynamics and turbulent structure. *J. Fluid Mech.* **780**, 60–98.

Li, Y., Perlman, E., Wan, M., Yang, Y., Meneveau, C., Burns, R., Chen, S., Szalay, A. & Eyink, G.L. 2008 A public turbulence database cluster and applications to study Lagrangian evolution of velocity increments in turbulence. *J. Turbul.* **9** (N31), 1–29.

Martin, J., Dopazo, C. & Valiño, L. 1998*a* Dynamics of velocity gradient invariants in turbulence: restricted Euler and linear diffusion models. *Phys. Fluids* **10**, 2012–2025.

Martin, J., Ooi, A., Chong, M.S. & Soria, J. 1998*b* Dynamics of the velocity gradient tensor invariants in isotropic turbulence. *Phys. Fluids* **10**, 2336–2346.

Meneveau, C. 2011 Lagrangian dynamics and models of the velocity gradient tensor in turbulent flows. *Annu. Rev. Fluid Mech.* **43**, 219–245.

Nomura, K.K. & Post, G.K. 1998 The structure and dynamics of vorticity and rate of strain in incompressible homogeneous turbulence. *J. Fluid Mech.* **377**, 65–97.

Ohkitani, K. & Kishiba, S. 1995 Nonlocal nature of vortex stretching in an inviscid fluid. *Phys. Fluids* **7**, 411.

Pumir, A. 1994 A numerical study of pressure fluctuations in threedimensional, incompressible, homogeneous, isotropic turbulence. *Phys. Fluids* **6**, 2071–2083.

SHE, Z.-S., JACKSON, E. & ORSZAG, S.A. 1990 Intermittent vortex structures in homogeneous isotropic turbulence. *Nature* **344**, 226–228.

SIGGIA, E.D. 1981 Numerical study of small-scale intermittency in three-dimensional turbulence. *J. Fluid Mech.* **107**, 375–406.

TAYLOR, G.I. 1938 Production and dissipation of vorticity in a turbulent fluid. *Proc. R. Soc. Lond.* A **164**, 15–23.

TIAN, Y., LIVESCU, D. & CHERTKOV, M. 2021 Physics-informed machine learning of the Lagrangian dynamics of velocity gradient tensor. *Phys. Rev. Fluids* **6**, 094607.

TOM, J., CARBONE, M. & BRAGG, A.D. 2021 Exploring the turbulent velocity gradients at different scales from the perspective of the strain-rate eigenframe. *J. Fluid Mech.* **910**, A24.

TSINOBER, A. 2009 *An Informal Conceptual Introduction to Turbulence*. Springer.

TSINOBER, A., ORTENBERG, M. & SHTILMAN, L. 1999 On depression of nonlinearity in turbulence. *Phys. Fluids* **11**, 2291–2297.

VIEILLEFOSSE, P. 1982 Local interaction between vorticity and shear in a perfect incompressible fluid. *J. Phys.* **43**, 837–842.

VIEILLEFOSSE, P. 1984 Internal motion of a small element of fluid in an inviscid flow. *Physica* A **125**, 150–162.

VLAYKOV, D.G. & WILCZEK, M. 2019 On the small-scale structure of turbulence and its impact on the pressure field. *J. Fluid Mech.* **861**, 422–446.

WILCZEK, M. & MENEVEAU, C. 2014 Pressure Hessian and viscous contributions to velocity gradient statistics based on Gaussian random fields. *J. Fluid Mech.* **756**, 191–225.

YANG, P.F., BODENSCHATZ, E., HE, G.W., PUMIR, A. & XU, H. 2023 Dynamics of the perceived velocity gradient tensor and its modeling. *Phys. Rev. Fluids* **8**, 094694.

YANG, P.-F., PUMIR, A. & XU, H. 2020 Dynamics and invariants of the perceived velocity gradient tensor in homogeneous and isotropic turbulence. *J. Fluid Mech.* **897**, A9.

YEUNG, P.K., SREENIVASAN, K.R. & POPE, S.B. 2018 Effects of finite spatial and temporal resolution on extreme events in direct numerical simulations of incompressible isotropic turbulence. *Phys. Rev. Fluids* **3**, 064603.

YEUNG, P.K., ZHAI, X.M. & SREENIVASAN, K.R. 2015 Extreme events in computational turbulence. *Proc. Natl Acad. Sci. USA* **112** (41), 12633–12638.

ZHOU, Z.D. & YANG, P.-F. 2023 Homogeneity constraints on the mixed moments of velocity gradient and pressure Hessian in incompressible turbulence. *Phys. Rev. Fluids* **8**, 024601.